

# Static and dynamic critical exponents in elastoplastic models of amorphous solids

E. E. Ferrero<sup>1</sup> and E. A. Jagla<sup>2</sup>

<sup>1</sup>*Instituto de Nanociencia y Nanotecnología, CNEA-CONICET, Centro Atómico Bariloche, (R8402AGP) San Carlos de Bariloche, Río Negro, Argentina.*

<sup>2</sup>*Centro Atómico Bariloche, Instituto Balseiro, Comisión Nacional de Energía Atómica, CNEA, CONICET, UNCUIYO, Av. E. Bustillo 9500 (R8402AGP) San Carlos de Bariloche Río Negro, Argentina*

We analyze the behavior of different elastoplastic models approaching the yielding transition. We establish a family of static universal critical exponents which do not seem to depend on the dynamic details of the model rules. On the other hand, we discuss that dynamical exponents are indeed sensitive to these details. We exemplify and discuss this fact by proposing two kind of dynamical rules for the local yielding events: occurring above the local threshold either at a uniform rate or with a rate that increases as the square root of the stress excess. The value of the flowcurve's (inverse) Herschel-Bulkley exponent  $\beta$  is seen to differ in  $\frac{1}{2}$  between these two cases. We give analytical support to this numerical observation by calculating the exponent variation in the Hébraud-Lequeux model and finding an identical shift. We further discuss an alternative mean-field approximation to yielding only based in the so-called Hurst exponent of the accumulated mechanical noise signal, which gives good predictions for exponents extracted from the simulations of the full spatial models.

## I. INTRODUCTION

The last years have witnessed major advances in the understanding of the deformation of amorphous solids from the statistical physics point of view [1, 2]. The so-called *yielding transition* between a solid-like and a flowing phase has been described and associated with both dynamical and equilibrium well known problems, as the depinning transition of elastic manifolds [3] and the random first-order transition in spin glasses [4]. In the seek of simplification and generalization, elastoplastic models (EPMs) built at a coarse-grained level constituted the workhorse in the development of such a description [5]. Nevertheless, the highly phenomenological approach on which these models have been built supplied a broad variety of rules and details, yielding different quantitative results and obfuscating the establishment of a set of universal exponents for the yielding transition. Despite a broad recent activity on the study of yielding by means of EPMs, universal properties remain elusive. Although some consensus has been built in the numerical community around the avalanche statistics displayed being different from mean-field depinning [5], quantitatively the reported critical exponents still differ. In particular, exponents such as the ones governing the flowcurve and the relation between avalanche size and duration show a wayward behavior. On the other hand, a comparison of EPMs with well known mean-field constructions and biased-random-walk problems, lead to a clearer expectation on where one would find universality and where model details should matter [6]. More importantly, experiments of yield-stress materials show themselves a broad variation of exponent values, e.g.,  $n \simeq 0.2 - 0.8$  for the Herschel-Bulkley exponent of the flowcurve [7]. More than an academic exercise, the forge of consensus around the critical properties of a problem is crucial in the practical development of the field. Is with that spirit that we address this issue.

In this work we contrast and analyze outputs from three different elastoplastic models previously used in the literature and further modify them to illustrate other three model cases. In particular, we focus in the modification of the rule that governs the onset of the increase of local plastic deformation, i.e., the local yielding. In general, when the local stress overcomes a preset threshold ( $\sigma_i > \sigma_i^{th}$ ) there is a probability  $\lambda$  per unit time that a plastic deformation occurs. In all versions of EPMs presented so far, the value of  $\lambda$  is taken as a constant. However, another alternative seems more natural. The plastic strain increase when the local stress threshold is overcome can be described as the passage between a local state that becomes unstable to a new stable state. Therefore, the typical time needed to move to the new minimum, and equivalently the transition rate  $\lambda$ , should be a function of the “degree of instability”  $\sigma_i - \sigma_i^{th}$ . We will call these “progressive rates”, as opposed to the constant or uniform ones. When this effect is quantitatively taken into account, the value of the inverse Herschel-Bulkley exponent of the flowcurve  $\beta$  ( $\beta \equiv n^{-1}$ ) is seen to differ in  $\frac{1}{2}$  between these two cases. We classify the exponents governing scaling laws in *static* and *dynamical* critical exponents, showing that while dynamical exponents, as  $\beta$ , may depend on the particular rules of the model (constant or progressive rates), static exponents are definitely universal. We illustrate with these two typical case rules replicated on each elastoplastic model analyzed. Furthermore, we support our numerical observation by estimating analytically the impact of the “progressive rates” modification in the paradigmatic Hébraud-Lequeux model. Our results offer a possible interpretation for the very broad range of experimental values observed in dynamical exponents of the yielding phenomenon.

In the athermal and overdamped limit in which the yielding transition is defined, the quasistatic dynamics is governed by *a priori* uncorrelated collections of plastic

events tagged avalanches. Events shaping an avalanche, in turn, are supposed to be correlated, giving rise to a non-trivial dynamics depending on interaction kernel and dimensionality. Yet, standing on a distant point of the system and assuming ergodicity, all the physics could be described by the mechanical noise felt by this point due to the avalanches taking place elsewhere. By analyzing the time series of the mechanical noise accumulated on time at a distant location, we can interpret our critical exponents from the problem of a biased random walk; e.g., giving an explicit expression for  $\beta$  in terms of the Hurst exponent of the accumulated mechanical noise signal, which constitutes in itself an alternative mean-field proposal for the study of yielding.

## II. MODELS AND SIMULATION PROTOCOLS

An amorphous material can be represented by a coarse-grained scalar stress field  $\sigma(\mathbf{r}, t)$ , at spatial position  $\mathbf{r}$  and time  $t$  under the application of a simple shear. Space is discretized in blocks (square lattice) and an over-damped dynamics is imposed for the stress on each block, following some basic rules: (i) The stress loads locally in an elastic manner while the block is “inactive” ( $n(\mathbf{r}) = 0$ ). (ii) When the local stress overcomes a local yield stress, a *plastic event* occurs with a given probability, and the block becomes “active” ( $n(\mathbf{r}) = 1$ ). Upon activation, dissipation occurs locally, expressed as a progressive drop of the local stress, together with a redistribution of the stresses in the rest of the system in the form of a long-range elastic perturbation. A block ceases to be active when a prescribed criterion is met. The auxiliary binary field  $n(\mathbf{r}, t)$  shows up in the equation of motion for the local stress  $\sigma(\mathbf{r}, t)$ , defining a dynamics that is typically non-Markovian. While the structure of the equation of motion for the local stresses is almost unique in the literature, both its parameters and the rules governing the transitions of  $n(\mathbf{r})$  ( $0 \rightleftharpoons 1$ ) show a variety of choices.

We define our EPMS as a 2-dimensional scalar field  $\sigma(\mathbf{r}, t)$ , with  $\mathbf{r}$  discretized on a lattice and each block  $\sigma_i$  subjected to the following evolution in real space

$$\frac{\partial \sigma_i(t)}{\partial t} = \mu \dot{\gamma}^{\text{ext}} - g_0 n_i(t) \frac{\sigma_i(t)}{\tau} + \sum_{j \neq i} G(i, j) n_j(t) \frac{\sigma_j(t)}{\tau}; \quad (1)$$

where  $\dot{\gamma}^{\text{ext}}$  is a global elastic loading,  $g_0$  is the local stress dissipation rate for an active site and the kernel  $G(i, j)$  is the Eshelby stress propagator [8].  $G(\mathbf{r}, \mathbf{r}') \equiv G(r, \phi) \sim \frac{1}{\pi r^2} \cos(4\phi)$  in polar coordinates, where  $\phi \equiv \arccos((\mathbf{r} - \mathbf{r}') \cdot \hat{\mathbf{r}}_{\dot{\gamma}^{\text{ext}}})$  and  $r \equiv |\mathbf{r} - \mathbf{r}'|$ . The last term in the RHS of 1 constitutes a *mechanical noise* acting on  $\sigma_i$  due to the instantaneous integrated plastic activity over all other blocks ( $j \neq i$ ) in the system. The picture is completed by a dynamical law for the local state variable  $n_i = \{0, 1\}$ . We define hereafter three different rules corresponding to three different models:

### 1. Picard’s model [9]

$$n_i : \begin{cases} 0 \rightarrow 1 & \text{at rate } \tau_{\text{on}}^{-1} & \text{if } \sigma_i > \sigma_Y \\ 0 \leftarrow 1 & \text{at rate } \tau_{\text{off}}^{-1} \end{cases} \quad (2)$$

where  $\tau_{\text{on}}$  and  $\tau_{\text{off}}$  are parameters and  $P(\sigma_Y) = \delta(\sigma_Y - 1)$ .

### 2. Lin’s model [2]

$$n_i : \begin{cases} 0 \rightarrow 1 & \text{at rate } \tau_{\text{on}}^{-1} & \text{if } \sigma_i > \sigma_Y \\ 0 \leftarrow 1 & \text{instantaneously} \end{cases} \quad (3)$$

where  $\tau_{\text{on}} = 1$  and  $P(\sigma_Y) = \delta(\sigma_Y - 1)$ . The plastic stress release is instantaneous and the block becomes inactive immediately after being activated, all  $j \neq i$  neighbors receive a kick that is proportional to the value of the local stress drop and mediated by the Eshelby propagator. The local stress drop value is chosen to be  $\sigma_i \pm \epsilon$ , with  $\sigma_i$  the local stress value just before yielding and  $\epsilon$  a uniformly distributed random variable with amplitude  $\epsilon_0 = 0.1$ , to avoid periodic dynamics effects.

### 3. Nicolas’ model [10]

$$n_i : \begin{cases} 0 \rightarrow 1 & \text{instantaneously if } \sigma_i > \sigma_Y \\ 0 \leftarrow 1 & \text{when } \int dt' |\partial_t \sigma(t') / \mu + \dot{\gamma}^{\text{pl}}(t')| \geq \gamma_c \end{cases} \quad (4)$$

here  $P(\sigma_Y)$  is exponentially distributed (as in [11]) and the integral over  $dt'$  accounts for the accumulated plastic deformation of the block after the last local yielding.

Besides their differences, one thing that these EPMS as-found-in-the-literature have in common is that they have a *fixed* or constant transition rate for plastic activation  $\lambda_{\text{fix}} = \tau_{\text{on}}^{-1}$ , be it finite or arbitrarily large as in Nicolas’ model. As already mentioned, a more natural alternative would be to associate a stress-dependent typical time with the passage between stable states. For example, by considering that the typical time  $t_0$  needed to move to a new minimum is a function of the degree of instability  $\sigma_i - \sigma_i^{\text{th}}$ . In particular, assuming a smooth form of the effective local potential energy on which the system evolves,  $t_0 \sim (\sigma_i - \sigma_i^{\text{th}})^{-1/2}$ . If we want to maintain an implementation in terms of transition rates,  $\lambda \equiv \tau_{\text{on}}^{-1}$  should be then expressed as  $\lambda \sim (\sigma_i - \sigma_i^{\text{th}})^{1/2}$ .

Notice that a situation of constant rate is recovered if the local potential is assumed to produce a jump in the force at the transition points, a situation that occurs, for instance, if the potential is formed by a concatenation of parabolas. In this case, the time it takes for the local stress to reach the new minimum when  $\sigma_i > \sigma_i^{\text{th}}$  is roughly constant, independent of the degree of instability. We can then associate the prescription of a constant

transition rate in previous EPMS to a local disordered potential formed by the concatenation of parabolic pieces (see further discussion in Sec. III F).

In summary, apart from the “classical” implementations of the three models described above, we further include in our present analysis the same three models but modified with stress-dependent transition rates of the kind  $\tau_{\text{on}}^{-1} = \lambda_{\text{prog}} = (\sigma_i - \sigma_{\text{Y}_i})^{1/2}$ . Other choices of  $\eta$  for  $\lambda_{\text{prog}} \propto (\sigma_i - \sigma_{\text{Y}_i})^\eta$  could be also considered. For any  $\eta > 0$  the intuitive expectation is that local regions that have exceeded their stress threshold by larger amounts will take precedence in their fluidization moment over others. As we will see, the change from  $\eta = 0$  to  $\eta = 1/2$  largely impacts the rheological properties of EPMS.

### Finite strain-rate protocol

Starting from an initial configuration  $\{\sigma_i\}$  that observes mechanical stability the system is evolved according to the equation of motion (1) with an elementary discretized time step  $dt = 10^{-2}$  (or smaller). After each time step integration of  $\sigma_i$ , the  $n_i$  are updated according to the corresponding rules (2,3 or 4, or one of their ‘progressive rate’ equivalents). The estimation of the stress increments in (1) is accomplished by computing the mechanical noise term in Fourier space to exchange a long-range interaction sum by a simple convolution. Our Es-selby propagator in Fourier space reads:

$$G_{\mathbf{q}} = -\frac{4q_x^2 q_y^2}{(q_x^2 + q_y^2)^2} \quad (5)$$

with the zero mode set as  $G_{\mathbf{q}=0} = -\kappa$  with  $\kappa = 1$ , unless specified; which results in  $g_0 \simeq 0.57$  in (1).  $q_x^2, q_y^2$  must be understood in a square numerical mesh of size  $L \times L$  as

$$q_{x,y}^2 \equiv 2 - 2 \cos\left(\frac{\pi m_{x,y}}{L}\right) \quad (6)$$

with  $m_{x,y} = 0, \dots, L - 1$ .

### Quasistatic protocol

Starting from any stable configuration, i.e., no site is active and no site stress is above its local threshold ( $n_i = 0$  and  $\sigma_i < \sigma_{\text{Y}_i}$  for all sites), the next avalanche of plastic activity is triggered by globally increasing the stress by the minimum amount necessary for a site to reach its local threshold. That site (the weakest) is activated at threshold with no stochastic delays; it perturbs the stress values of other sites and the rest of the avalanche evolves without any external drive. In fact, it does it following the same dynamics established by Eq. (1) (and the corresponding activation rule) at  $\dot{\gamma} = 0$ . When no site is active or able of being activated

( $\sigma_i > \sigma_{\text{Y}_i}$ ) the avalanche stops and the loading process is repeated.

We have noticed that Nicolas’ model as originally proposed [10] is ill-defined in the quasistatic protocol. Eventually one arrives to the pathological case in which a site is active and the criterion to recover local elasticity (4) is never met (any finite  $\dot{\gamma}$  guarantees it, but not the quasistatic protocol). To overcome this issue, we add a maximum duration bound to plastic events, yet large enough to guarantee the full relaxation of the local stress.

## III. RESULTS

### A. Flowcurves

To build flowcurves we use the strain rate controlled simulation protocol. We first deform with a large strain rate (e.g.  $\dot{\gamma} \simeq 0.5$ ) until a global steady stress value is reached, and then average it in time. Then the strain rate is reduced and the protocol is repeated, covering a proper range in strain rates to draw the flowcurve in log-scale.

When arriving from the “fluid” side the approach to the yielding point is continuous and the transition is critical. As the strain rate  $\dot{\gamma}$  vanishes, the average stress reaches a finite value that we call the (dynamical) yield stress  $\sigma_c$ . In the vicinity of the limit  $\dot{\gamma} \rightarrow 0$  the flowcurve obtained by a strain rate control protocol  $\langle \sigma(\dot{\gamma}) \rangle = \sigma_c + A\dot{\gamma}^\beta$  can be also written as

$$\dot{\gamma} \propto (\langle \sigma(\dot{\gamma}) \rangle - \sigma_c)^\beta, \quad (7)$$

where  $\beta = 1/n$ .

Fig. 1 displays flowcurves for all three EPMS with both constant and progressive transition rates for local yielding. While the upper panel displays average stress vs. strain rate, in the lower panel we plot the strain rate as a function of the stress excess above the dynamical yield stress. One important detail in the construction of these curves is the appropriate estimation of  $\sigma_c$ , for which we have implemented separately quasistatic measurements and averaged the stress in this limit over long deformation windows. Although it is a delicate fitting procedure, not free from finite-size effects, once  $\sigma_c$  has been properly determined, all EPMS with uniform rate show a flowcurve exponent compatible with  $\beta = 3/2$ , as for the depinning-like models with piece-wise parabolic disorder potential [12]. Interestingly, when progressive rates are used instead, the exponent changes to  $\beta = 2$  in all the three models taken from the literature; suggesting that a local fluidization rate of the form  $\lambda_{\text{prog}} = (\sigma - \sigma_{\text{Y}})^{1/2}$  takes us to the case of ‘soft’ disorder potentials [12]. In any case, Fig.1 clearly shows that the particular dynamical rule that is used for local yielding has a direct impact in the value of the flowcurve exponent.

It can be noticed in passing that, by using progressive rates, the exponent obtained in our  $2d$ -systems is  $\beta = 2$ , as the one derived for the mean-field Hébraud-Lequeux

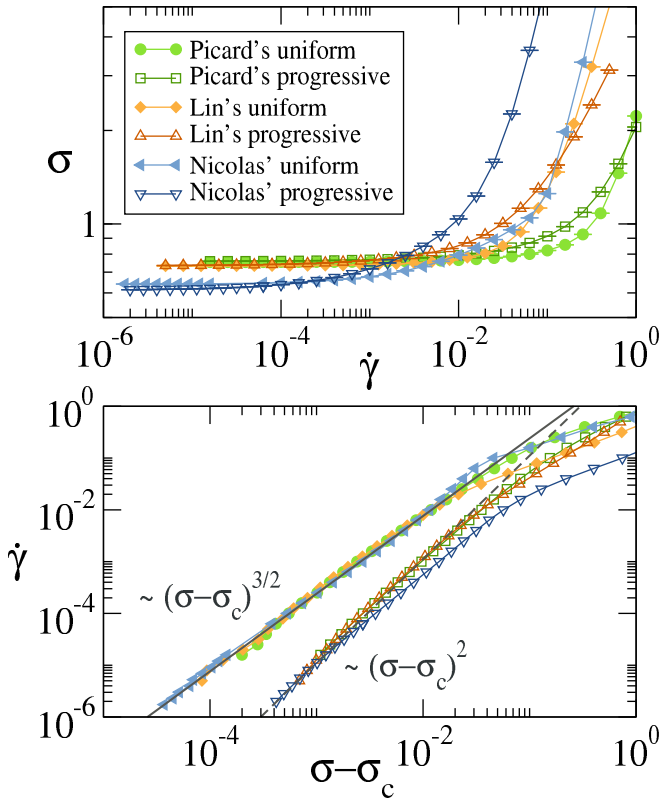


Figure 1. Flowcurves for different elastoplastic models. Data corresponding to each model variant is identified by symbols and colors as in the legend. System size is  $N = 2048^2$ . *Upper panel*: stress  $\sigma$  vs. strain rate  $\dot{\gamma}$ . *Lower panel*: strain rate  $\dot{\gamma}$  vs. stress excess  $\sigma - \sigma_c$  (curves shifted arbitrary in the vertical direction for comparison). Straight lines corresponding to power-law exponents  $\beta = 3/2$  and  $\beta = 2$  are also displayed.

(HL) model [13, 14]. Nevertheless, in the HL model the activation rate is constant. The reason for this accidental coincidence rests in the fact that the flowcurve exponent is not only determined by the transition rates, but also by the mechanical noise statistics (which is dimension-dependent), as discussed later on.

## B. Quasistatic avalanche distributions

Starting from a system that has been deformed at a slow strain rate, we apply a quasistatic protocol. Size  $S$  and duration  $T$  of each triggered avalanche are measured.  $S$  is simply estimated from the total stress drop  $\Delta\sigma$  caused by the avalanche of plastic events as  $S = \Delta\sigma L^d$ , while  $T$  is the time elapsed until the avalanche ceases its activity, measured in units of  $dt$ .

Figure 2 shows avalanche size distributions for all three models in their two transition rate variants, at various system sizes. All distributions have the form  $P(S) \sim S^{-\tau} f(S/S_{\max})$ , with  $f(x)$  a rapidly decaying function (a compressed exponential). Taking a single EPM no

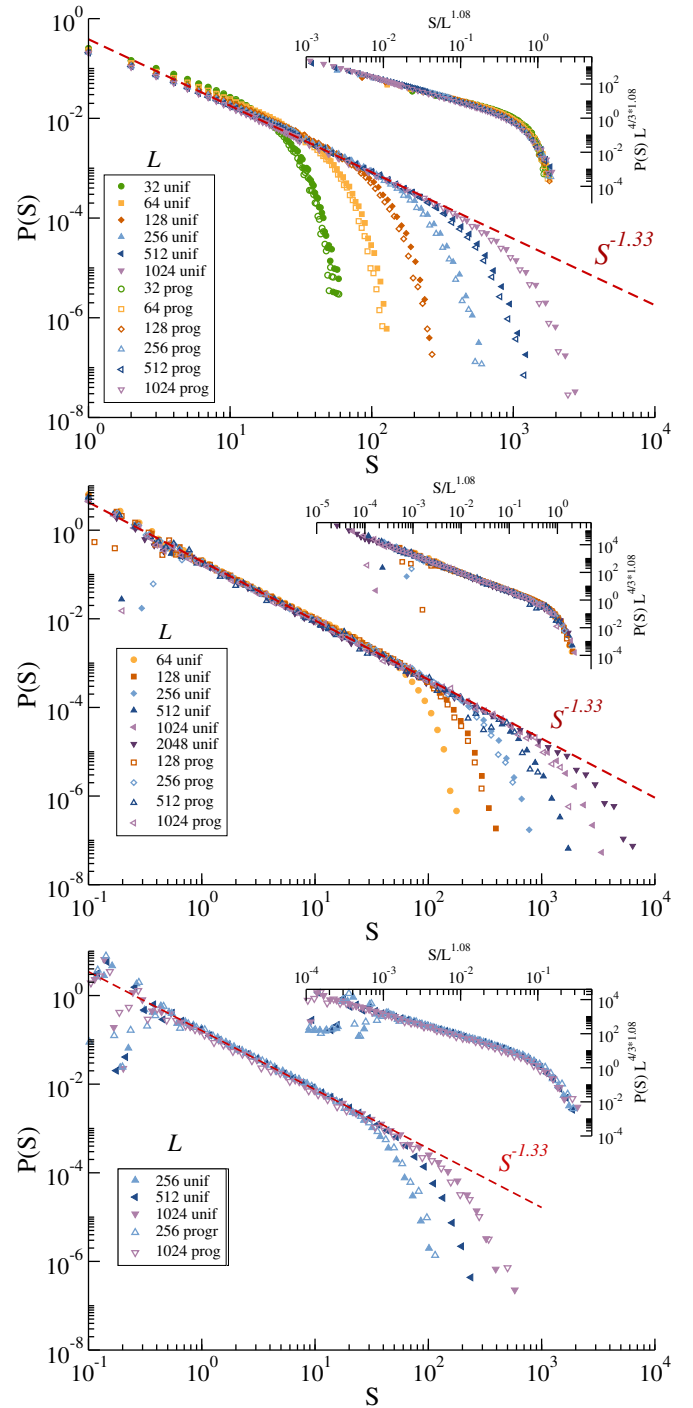


Figure 2. Avalanche size distribution of the quasistatic dynamics for different system sizes as described by the legends. *Upper panel*: Lin's model. *Middle panel*: Picard's model. *Lower panel*: Nicolas' model. For each model, results of simulations corresponding to uniform (filled symbols) and progressive (open symbols) yielding rates are shown. On each panel, the dashed line displays a power-law  $\sim S^{-\tau}$  with  $\tau \simeq 1.33$ . Inset shows the scaling  $P(S)L^{\tau d_f}$  vs.  $S/L^{d_f}$ , with  $d_f \simeq 1.08$ ,  $\tau \simeq 1.33$ .

difference between uniform and progressive rates is observed. Furthermore, the same value of  $\tau \simeq 1.33$  characterizes all avalanche distributions, irrespective of the six model variants analyzed. Good collapses of the distributions for different system sizes is found when plotting  $P(S)L^{\tau d_f}$  vs  $S/L^{d_f}$  with the so-called ‘‘fractal dimension’’  $d_f = 1.08$ . However, explicit and acceptable fittings of  $P(S) = AS^{-\tau} \exp(-(S/S_{\max})^b)$  with  $b \simeq 1.5 \dots 2$  may result in  $S_{\max} \propto L^{d_f}$  with  $d_f \simeq 1.1 \dots 1.5$  as well. In any case, we notice that  $d_f$  is independent on the particular form of the rates used.

Apart from the arbitrariness in the determination of  $d_f$  a word should be said about the accurate quantitative estimation of  $\tau$ . We have noticed that, even when it moves on a limited range, this exponent may be sensitive to some technicalities of the simulation. For example, the avalanche distribution may change with the parameter of stress (non-)conservation  $\kappa$  (the value chosen for  $-G_{q=0}$ ). We know that when  $\kappa = 0$  stress is conserved by the dynamics. In this case, we will eventually have a never ending avalanche (once the loading phase takes us above the critical threshold). Therefore, different values of  $\kappa$  are set, being  $\kappa = 1$  the most commonly used in ‘‘strain-preserved’’ simulations and the one we adopted in general for this work. Fig.3 illustrates for Lin’s model (with uniform rates) how this choice affects the quantitative estimation of  $\tau$ , changing from  $\tau \simeq 1.33$  for  $\kappa = 1$  to  $\tau \simeq 1.25$  for  $\kappa = 0.01$ , and may justify the dispersion of exponent values found in the literature [2, 5, 11, 15, 16]. Furthermore, this effect is intrinsically related with the variability of  $\tau$  observed in numerical simulations of a mean-field model for yielding as discussed in [17].

As a partial conclusion,  $\tau$  and  $d_f$  appear to be universal exponents independent of the particular model once a simulation protocol is defined. Yet, their quantitative

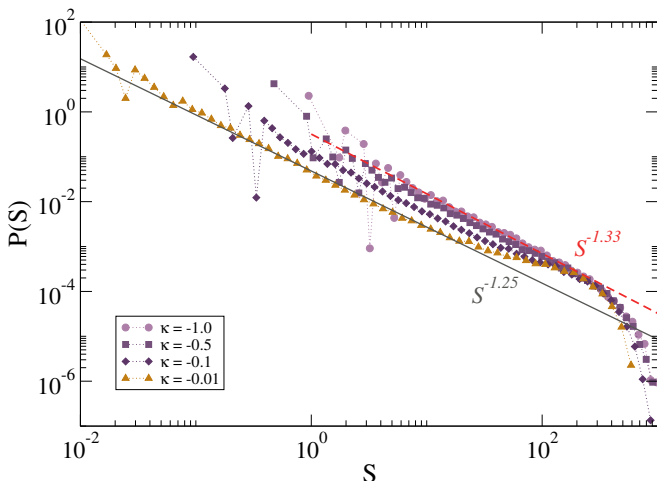


Figure 3. Avalanche size distribution of the quasistatic dynamics of Lin’s model with uniform rates for system size  $N = 512^2$  and different choices of the stress non-conservation parameter  $\kappa$ .

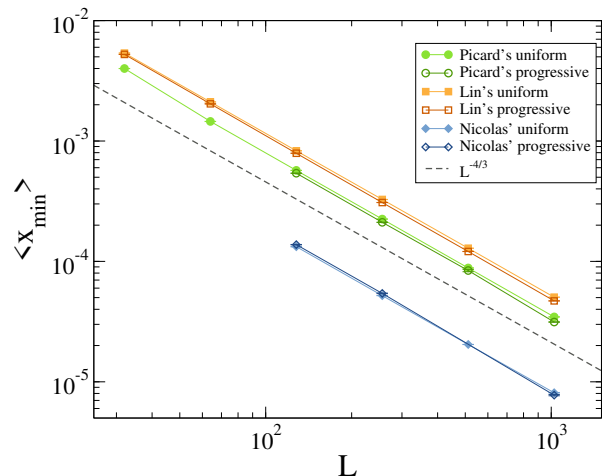


Figure 4. Finite size scaling of the average stress needed to trigger a new avalanche  $x_{\min}$  for all model variants, as indicated by the legend. The dashed line shows  $\sim L^{-4/3}$  for comparison.

estimation may depend on protocol details.

### C. Extremal statistics and density of shear transformations $P(x)$

Directly related to the avalanche size statistics is the stress  $x_{\min}$  needed to trigger the next avalanche each time ( $x_{\min} = \sigma_{Yw} - \sigma_w$ , where  $w$  stands for the ‘‘weakest’’ site). It was first observed by molecular-dynamics simulations [18] and then contextualized in a framework of extreme statistics both in MD [1] and EPMS [2], that the finite size scaling of the average loading stress needed to trigger avalanches is sub-extensive, i.e.,

$$\langle x_{\min} \rangle \propto N^{-\phi}, \quad \text{with } 1 < \phi < 2 \quad (8)$$

with  $N = L^d$ . This is at odds with the intuition that we get from analogies with sand-pile models or other stick-slip dynamics as the one related to the depinning transition. There, the intensive local variables (pile height or force at site  $i$ , equivalent to the stresses  $\sigma_i$ ) can only increase as the intra-avalanche dynamics proceeds and therefore a larger system will always show an equally weaker site on average ( $\phi = 1$ ).

This phenomenological sub-extensiveness was interpreted as a consequence of marginal stability in the driven amorphous solid by Lin *et al.*[2]; In average, starting at any given steady state configuration, sites far away from their thresholds have a much larger life time before yielding than sites that are close to it. Since plastic activity provides signed kicks to each site stress, the problem of local yielding is that of a first passage time, and the probability of finding the walker somehow away from the boundary is much larger than finding it very close to it. Analyzing the distribution  $P(x)$  of local stresses

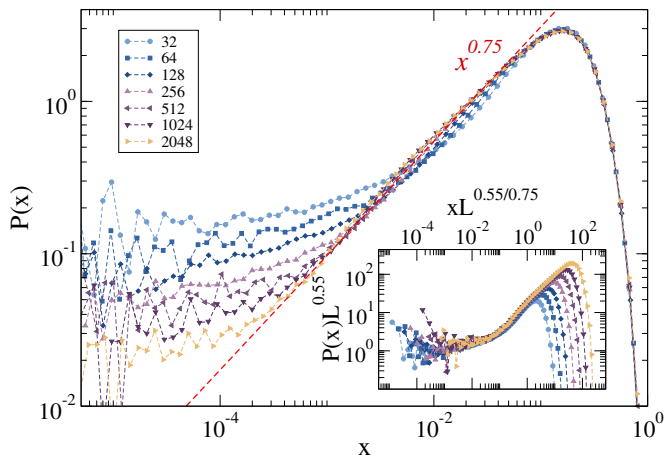


Figure 5.  $P(x)$  for different system sizes as indicated in the labels corresponding to Picard’s model with uniform rates. The inset shows the scaling  $P(x)/L^{-a}$  vs.  $x/L^{a/\theta}$ , with  $a = 0.55$ .

needed to reach local thresholds ( $x_i = \sigma_{Y_i} - \sigma_i$ )-tagged the “density of shear transformations”- and assuming it to be characterized by a power-law  $P(x) \sim x^\theta$  at small  $x$ , it can be shown that the distribution of the minimal values ( $x_{\min}$ ) among randomly chosen sets of  $N \gg 1$  independent samples from  $P(x)$  is a Weibull distribution with mean value

$$\langle x_{\min} \rangle \sim N^{-1/(1+\theta)} = L^{-d/(1+\theta)}. \quad (9)$$

In this way, any  $\theta > 0$  provides a sub-extensive  $\langle x_{\min} \rangle$ , and in fact,  $\theta > 0$  was estimated [1, 2, 5] for the yielding of amorphous solids in contrast with the  $\theta = 0$  value of the depinning of elastic manifolds. Fig. 4 shows  $\langle x_{\min} \rangle$  as a function of system size for different elastoplastic models. We can observe that results for the uniform and progressive rates variants of the models are totally consistent. Furthermore, all the simulated EPMS display the same scaling law  $\langle x_{\min} \rangle \sim L^{-1.33}$ , compatible with  $\theta \simeq 0.5$  in Eq.9.

At this point, it is appropriate to clarify a dichotomy in the determination of exponent  $\theta$ . It turns out that  $\theta$  determined from Eq.9 (and Fig.4) and  $\theta$  estimated from a power-law fit of  $P(x)$  do not necessary coincide. In Fig.5 we show the form obtained for  $P(x)$ . The deviation from a common power law, and the establishment of a system-size dependent plateau at  $x \rightarrow 0$  is clear, as it is also the fact that this plateau occurs systematically at smaller values of  $x$  as  $L$  increases.  $P(x)$  preserves the excess of probability at  $x = 0$  even when the  $x$  values are rigorously collected just after the end of an avalanche and before the next loading stage. Notice that this effect can be easily overseen if an arbitrary lower cutoff of the histograms is imposed. At the same time, the limited power-law range facilitated by relative small system sizes, as is usually the case, does not help to catch a clear value for  $\theta$ . In our case, only when  $L$  is big enough we

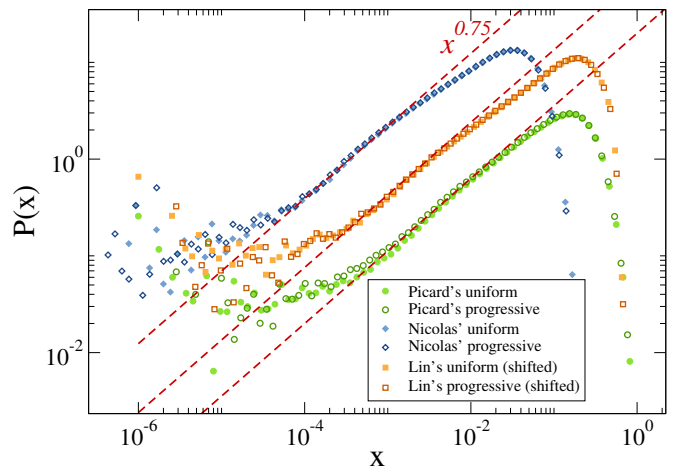


Figure 6.  $P(x)$  for different model variants as indicated in the labels and Red dashed lines display  $\sim x^\theta$  with  $\theta \simeq 0.75$  to guide the eye. System size is  $N = 1024^2$  in all cases.

can start to see that  $P(x)$  displays a power-law in more than a decade with exponent  $\theta \simeq 0.75$ , before saturating to a plateau at  $x \rightarrow 0$ . A priori, we interpret the plateau effect at small  $x$  as a consequence of working with a discrete time step in the dynamics, in analogy with the same phenomenon occurring for discrete time random walks in the presence of an absorbing border: the probability amplitude right at the border is finite and its value decreases with the amplitude of the time step. Yet, we have performed simulations with time steps down to  $dt = 10^{-4}$  and the modification of the obtained  $\langle x_{\min} \rangle$  values is very slow. The true origin of the finite size scaling for the  $P(x)$  plateau at  $x \rightarrow 0$  remains elusive to us. The inset of Fig.5 simply show an empirical scaling assuming that, at least in the discrete model,  $P(x) = P(0) + x^\theta$  with  $P(0) \sim L^{-a}$ .

In Fig.6 we plot  $P(x)$  for different models with  $L = 1024$ . The values of  $\theta$  that one could obtain from such curves vary between 0.56–0.77 according to the criterion used to identify the power-law regime. Yet, in any case, the extracted exponent value is independent on each activation rate used, as the correspondent distributions for the same model lay one above the other. Furthermore, for all model variants we see a good compatibility with  $\theta = 0.75$ , assuming  $P(x) \sim x^\theta$  in the (still arbitrary) range of small values of  $x$  just before the asymptotic saturation for  $x \rightarrow 0$ .

It could be argued that being an effect that decreases with system size, the plateau in  $P(x)$  for small  $x$  must eventually become irrelevant: for sufficiently large system sizes the full  $P(x)$  would acquire the expected  $P(x) \sim x^\theta$  form, and the scaling in Eq. 9 would hold. But this is not so. Comparing values of  $x_{\min}$  in Fig. 4 with the full distribution of  $P(x)$  in Fig.5 we see that  $x_{\min}$  is always in the plateau region of  $P(x)$ , and then it is the scaling of this plateau with system size what determines the values reported in Fig. 4. Thinking the other way around, we do

not find any strong reason why the value of  $\theta$  determined from Fig. 4 should be equal to the asymptotic form of  $P(x)$  (the red dashed line in Fig. 5). In fact, these values do not coincide as far as we can tell: while from Fig. 4 we obtain  $\theta \simeq 0.5$ , the value from the asymptotic form in Fig. 5 is rather  $\theta \simeq 0.75$ . Actually, this situation is not new in the literature, where  $\theta \sim 0.45 - 0.5$  has been determined from the scaling of  $x_{\min}$  but larger values ( $\theta \simeq 0.6$ ) have been obtained from the full  $P(x)$  in two-dimensional systems [1, 2, 5]. Besides a lack of a better understanding of the difference in the values of  $\theta$  determined by the two different methods, it should be kept in mind that the exponent ruling the dynamics in the quasistatic limit is the one obtained from  $\langle x_{\min} \rangle$  (Fig. 4) since this is the average value of stress that is actually added to the system after each avalanche to keep the system state stationary. On the other hand, it is the value of  $\theta$  extracted from  $P(x)$  the one that is related with the flowcurve exponent [19] (see also Sec.III F).

#### D. Avalanche durations

We now consider the second exponent for which a dependence on the rate law may be expected. This is the dynamical exponent  $z$  that, combined with  $d_f$ , relates the avalanche size with the avalanche duration. The avalanche duration  $T$  is expected to scale as a power law of the avalanche size  $S$ , namely  $T \sim S^{1/\delta}$ . If we assume that both  $S$  and  $T$  are controlled by a correlation length  $\ell$  through  $S \sim \ell^{d_f}$  and  $T \sim \ell^z$ , then  $T \sim S^{z/d_f}$  and  $\delta = d_f/z$ .

Fig.7(top) shows the  $T$ - $S$  relation for a large set of avalanches of quasistatic simulations at a fix system size ( $L = 1024$ ) from Lin's model with both constant and progressive rates. We can observe for both cases a broad cloud of points, but clearly different for different rate rules. Although scaling relations are difficult to guess from these clouds, it is clear that the progressive rate allows for a much larger spread of avalanche durations for the same avalanche size, in particular, it allows for avalanches much longer in time. Now, averaging the values of  $T$  within small  $S$  intervals, for different system sizes we obtain the curves in Fig.7(bottom). For uniform rates, the results show a consistent power law with an exponent  $z/d_f \simeq 0.54$ . Data for all system sizes overlap on the same curve. Using the previously determined value  $d_f \simeq 1.08$ , we can obtain  $z \simeq 0.58$ . For progressive rates, the results are definitely different. At a fix system size, a grow of  $\langle T \rangle$  vs  $S$  with exponent  $z/d_f \simeq 0.43$  is established for large enough avalanches, yielding for the dynamical exponent  $z \simeq 0.46$ , i.e., lower than the uniform case. Even more, an additional behavior is observed. The results for increasingly large system sizes do not simply extend the region in which a power law is observed but also produce a shift of the average duration towards larger values.

This unexpected result can be rationalized in the fol-

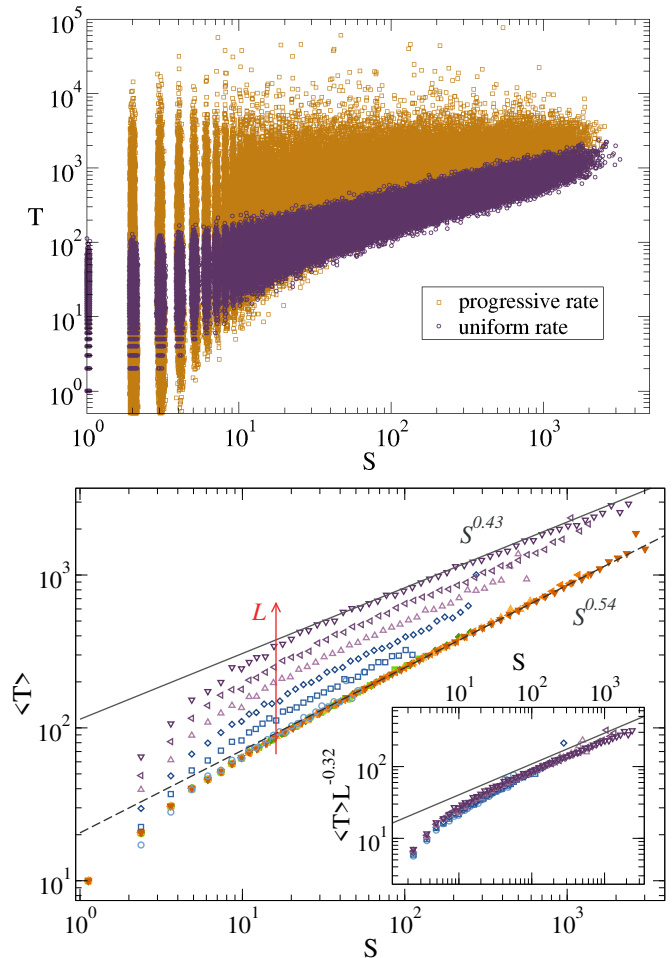


Figure 7. *Top panel:* Scatter plot of avalanche duration  $T$  vs size  $S$  for Lin's model with uniform and progressive rates (linear system size  $L = 1024$ ). *Bottom panel:* Averaged avalanche duration as a function of the avalanche size for Lin's model with uniform and progressive rates and different linear system sizes  $L = 32, 64, 128, 256, 512, 1024$ . The inset shows the scaling proposed in Eq.10 and derived in Appendix A.

lowing way. Each time an avalanche triggers a new plastic event, its life is expanded and some time will be added to its final duration. For uniform activation rates, this time is on average  $dT = \lambda^{-1} = 1$ . On the other hand, for progressive rates, the time added to the avalanche duration depends on the stress excess of the new yielding site; on average  $dT = \lambda^{-1} = (\sigma_i - \sigma_{Y_i})^{-1/2}$ . The events that most contribute to the avalanche duration then, are the ones that occur very close above their threshold. While their individual probability of yielding is low, the observation of these events increases with the number of sites susceptible of being in that situation; this is, it increases with increasing system size. This previously unnoticed phenomenon is also present at a mean-field level, where a more quantitative estimation of the value of  $z$  can be given and an exact scaling law derived (see Appendix A), leading to the  $N$  and  $S$  dependence of the avalanche du-

ration:

$$T \sim N^\alpha S^{(1-\alpha)/2} \quad (10)$$

We have tested this scaling in the inset of Fig. 7(bottom), and it works very well with  $\alpha \simeq 0.16$ .

Notice that in the numerical determination of the durations  $T$  reported in this section, the time needed to destabilize the first site in the avalanche was not considered. This was chosen in this way since, as the first site is destabilized by an infinitesimal quantity, it would add a diverging contribution to the total time when progressive rates are at play, completely spoiling the duration estimation. For uniform rates the first site only adds an additional time unit, but for consistency we don't consider it either in this case.

To conclude this section, let us include a brief digression about dynamical critical exponents. Since the instantaneous long-range interaction is responsible for the dependence on microscopic properties and ultimately, for the different values of  $\beta$  and  $z$  found, one can argue (as Lin and Wyart [20]) that spurious effects will disappear when this ‘unphysical’ instantaneous interaction is eliminated (by adding a mechanism for propagating waves, for example). While this might probably be case, the use of instantaneous interaction is not necessarily an unphysical assumption that should be improved, but rather makes sense in many different physical systems when restricted to the appropriate spatial and temporal scales. In the depinning of magnetic structures for instance, long-range interactions (typically dipolar) are considered, although these interactions cannot travel faster than the speed of light! Also, the problem of contact line depinning is known to have a long-range elastic interaction decaying as  $1/r^2$ . This interaction is generated through the elastic propagation of interactions in the bulk of the material, and in the end its propagation velocity cannot be instantaneous but must be limited to the speed of sound in the material. Nevertheless, that finiteness for the elastic propagation velocity has not been a major obstacle for the theory there. In our case, an Eshelby instantaneous interaction is an approximation that consider the speed of sound in the system to be infinite. This is clear for instance in the analysis of Cao *et al.* [21], where in order to derive the Eshelby interaction an infinite bulk modulus –and thus an infinite sound velocity– is considered. This approximation produces some results that cannot be correct in a more realistic situation. For instance a value of the dynamical exponent  $z$  lower than one indicates a propagation of perturbations as  $r = Ct^{1/z}$ , and thus at velocities larger than any finite value if considering sufficiently large times or distances. The consideration of a finite sound velocity  $c_s$  must provide ultimately a value of  $z \geq 1$ . Yet the values we find for  $z$  and  $\beta$  and, furthermore their different values for different dynamical rules, still make sense if we are analyzing cases (avalanche durations and sizes, for instance) for which  $r/t = Ct^{1/z-1} = C^z r^{1-z} \ll c_s$ .

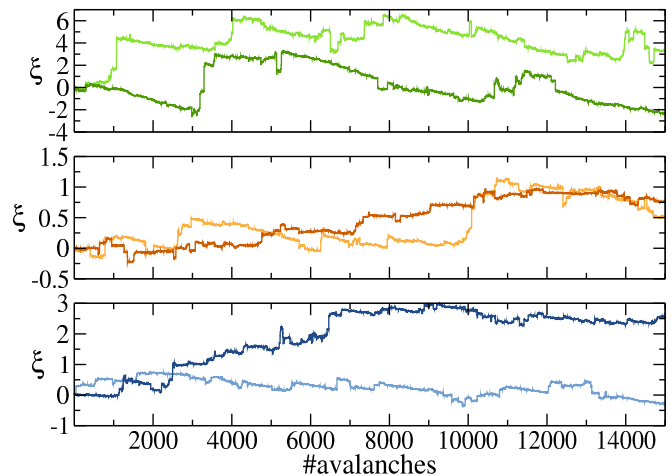


Figure 8. Different realizations of the accumulated mechanical noise  $\xi$  as a function of a quasistatic ‘‘time’’ represented by the number of avalanches for Picard’s (top panel), Lin’s (mid-panel) and Nicolas’ model (bottom panel) with both uniform (light colors) and progressive (dark colors) rates, and  $L = 256$ .

### E. Accumulated mechanical noise

Although it has been reported in the literature that some critical exponents are dimension-dependent, the long-range nature of the Eshelby interaction kernel makes us believe that the yielding transition would support an effective mean-field description, as soon as we correctly choose the distribution for a plugged mechanical noise in each finite dimension. Standing on an arbitrary site  $i$  in the system we can define  $\xi_i(t)$  as the accumulated mechanical noise on  $i$  at time  $t$  due to avalanches occurring elsewhere. We would like to study the statistical properties of this noise and relate it to the observed values of the avalanche statistics and the rheological exponent  $\beta$ . In particular, we are interested in describing  $\xi(t)$  as a correlated noise with statistical properties defined by the so-called Hurst exponent  $H$ , so that  $\xi(x)$  is an homogeneous function of degree  $H$ ,

$$\xi(kx) = k^H \xi(x) \quad (11)$$

Note that a standard random walk (uncorrelated noise) has  $H = 1/2$ . In general, in a mean-field description [19],  $H = 1/\mu$  where each contribution  $\delta\xi$  to the accumulated noise  $\xi$  is assumed to come from a distribution with a long tail

$$P(\delta\xi) \sim \frac{1}{|\delta\xi|^{\mu+1}} \quad (12)$$

Taking into account the action of individual plastic events through the Eshelby propagator, Lin and Wyart [19] arrived to the conclusion that  $\mu = 1$  was the only value with ‘‘physical’’ sense. Nevertheless, if we discretize time in such a way that we can see the occurrence of

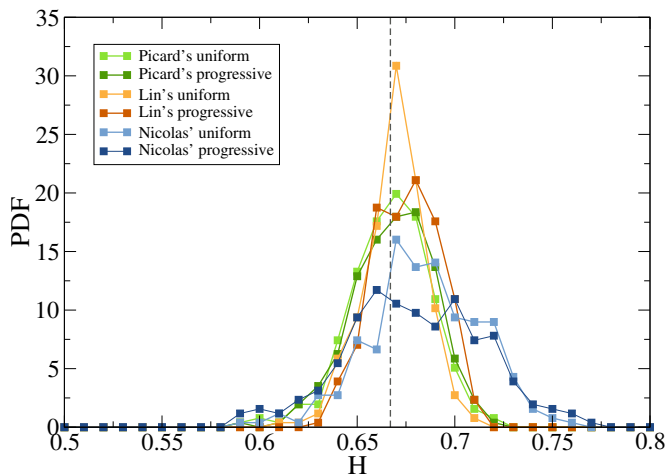


Figure 9. The Hurst exponent analysis of all EPMs models in their two variants. Histograms are built from the  $H$  values obtained from accumulated noise signals taken at 256 different points in systems of size  $N = 256^2$ . The vertical dashed line corresponds to  $H = \frac{2}{3}$ .

avalanches as the elementary event contributing to the mechanical noise, other values of  $\mu$  may acquire a physical sense. In fact, a distant site at a given moment in the relevant time scale does not feel the mechanical kick produced by a single site, but by a full avalanche of sites yielding. A coarse-graining in time is done by the system itself, which does not necessary constraint the plastic events to occur one at a time and well separated but overlaps them in sudden burst of activity. In a quasistatic loading protocol, the time scale separation between the duration of one avalanche and the loading time to trigger the next one allows us to make this approximation and set the time-scale in avalanches count.

Figure 8 displays different realizations of  $\xi$  for various of our EPMs. We can already notice with the bare eye the characteristic long steps or Lévy flights that distinguish this kind of signal from random-walks. More importantly, we will show that in all cases these signals show values of  $H$  that are very close to each other, pointing to a robust value of  $H$  that defines an intrinsic property of the system. To compute  $H$  we can analyze the signal in the following way: for each window of size  $\epsilon$  in the avalanche sequence compute the average value of the absolute noise difference in that window  $\langle \delta \rangle(\epsilon) = \frac{1}{M} \sum_i^M |\xi(i) - \xi(i+\epsilon)|$ .  $H$  is then the exponent of the relation  $\langle \delta \rangle \sim \epsilon^H$ . This is basically what the Detrended Fluctuation Analysis (DFA) (Nolds [22]) does after having subtracted from the signal a global trend. Therefore, we collect large series of the accumulated mechanical noise at different points in the system and analyze these signals with the DFA algorithm. Results for the histograms of  $H$  values observed are shown in Fig. 9 for the different models and rate rule variants. We observe that all systems show some spread around a mean value  $\sim 0.67$ , but already the concurrence

of all model variants around such a particular value is non-trivial. The DFA analysis is sensitive to details as the total signal length and the minimum segment length for polynomial fitting, installing a non negligible uncertainty in its output. We believe that a good theoretical proxy for the Hurst exponent in 2d-EPMs is  $H \simeq \frac{2}{3}$ , signaled by a vertical dashed line in Fig. 9. This corresponds to  $\mu = \frac{1}{H} \simeq 1.5$  in Eq. 12, subscribing the idea that a coarse-graining in time can give a physical meaning to values of  $\mu$  different from  $\mu = 1$ . The Hurst exponent is independent on the rate rule, what puts it at the level of other static critical exponents such as  $\tau$ ,  $\theta$  or  $d_f$ . We further confirm that the exponent  $H$  characterizing the mechanical noise in a quasistatic measure is key for the estimation of the  $\beta$  exponent of the flowcurve as it departs from the critical yielding point, as discussed in the following section.

## F. Relations among exponents

In this section we recall and discuss some scaling laws present in the literature. To start with, an interesting relation among exponents comes from a very simple argument originally presented by Lin *et al.* [2]. In the steady state, the stress has a well defined average and describes a jerky plateau as a function of strain for any finite system size. Therefore, on average, the stress increases in the loading phases must be balanced by the stress drops during avalanches. From the avalanches distributions  $P(S) \sim S^{-\tau} f(S/L^{d_f})$ , with  $f(y)$  a fast decaying function for  $y \gg 1$  and considering  $S \equiv \Delta\sigma L^d$ , one obtains  $\langle \Delta\sigma \rangle \propto L^{d_f(2-\tau)-d}$ . On the other hand, the stress increment needed to trigger a new avalanche is what we have called  $x_{\min}$  which scales as  $\langle x_{\min} \rangle \propto L^{-\frac{d}{\theta+1}}$ . Equating  $\langle \Delta\sigma \rangle \propto \langle x_{\min} \rangle$ , leads to

$$\tau = 2 - \frac{\theta}{\theta+1} \frac{d}{d_f}. \quad (13)$$

By considering the values of  $\theta \simeq 0.5$  taken from Fig.4 and  $\tau \simeq 1.33$  and  $d_f \simeq 1.08$  from Fig.2, this relation fairly holds for our data. This is not surprising since, as we explained, Eq. 13 is originated in a simple requirement of stress stationarity in the system. Note however that Eq. 13 is not satisfied using the  $\theta$  value obtained from our data when considering the distribution  $P(x) \sim x^\theta$ .

When dynamical exponents enter into the discussion things are less clear. Different relations have been proposed in the literature, in particular  $\beta = 1 + \frac{z}{d-d_f}$  [2],  $\beta = 1 + \frac{1}{d-d_f}$  [20], that show either a weak agreement with simulations or an asymptotic agreement in dimensions higher than  $d = 3$ . We believe that this attempts originated somehow in the fact that the mean field prediction [19]

$$\theta = \mu/2 \quad (14)$$

was not accompanied by good numerical evidence in finite dimension EPMs. Our data, on the contrary, shows that

this relation holds; of course, as soon as we accept a mean-field construction with an effective ruling exponent  $\mu = 1/H$ .

Following [19, 20], what we call  $\mu$  here is the exponent governing the fat tails of the mechanical ‘kicks’  $\delta\xi$  distribution

$$w(\delta\xi) = \frac{A}{N} |\delta\xi|^{-\mu-1} \quad (15)$$

with appropriate cutoffs. Further notice that the exponent  $\mu$  happens to be exactly equal to the  $\beta$  exponent governing asymptotically the flowcurve in the same analytical approach [19, 20]. Still, rather than believing that those kicks come from individual uncorrelated plastic events, we assume that they come from spatially correlated objects (avalanches) occurring elsewhere in the system. Therefore,  $\mu$  turns to be an effective exponent, eventually depending on system dimension, the fractal dimension of those objects and their distribution. Adopting that idea we have gone through the path of estimating  $\mu$  (or  $H$ ) from the simulations (Sec. III E) and the values yielded turned out to be consistent with the ones of the flowcurve and the following relation (to be justified below)

$$\theta = \frac{\mu}{2} = \frac{1}{2H} = \frac{1}{2} \left( \beta - 1 + \frac{1}{\omega} \right). \quad (16)$$

where,  $\omega$  is related to the analytical form of the disorder potential between consecutive wells:  $\omega = 1$  for concatenated parabolae potentials (uniform rates) and  $\omega = 2$  for sinusoidal or ‘smooth’ potentials (progressive rates).

Concerning Eq. (16), let us first remark that in the common case of parabolic potentials (uniform rates,  $\omega = 1$ ) the equation above reduces to  $\theta = \beta/2$ ; [23] an extremely simple relation between the flowcurve exponent and the power exponent of the density of shear transformations in the steady state in the quasistatic limit that makes perfect sense: The steeper the  $P(x)$ , the sooner many sites will yield when we set the system in motion, the faster strain rate will increase and (equivalently) the slower the global stress will increase with  $\dot{\gamma}$  due to the frequency of local fluidization. Notice that such a simple expression is also valid for the HL model ( $\beta = 2$ ,  $\theta = 1$ ).

We now justify Eq. 16 finding footing in previous works. In [12], the relation of EPMS and models *à la* depinning, which make use of a quenched disordered potential was discussed. Basically, the system described by the local stress evolution (1) and the complementary rules for the scalar  $n$  of local activity can be replaced by a system in which the natural variable is the local deformation  $e_i$  subject to an equation of the form

$$\dot{e}_i = \tilde{\mu}(\gamma_i^{\text{pl}} - e_i) + \sum_j G_{ij} e_j + \sigma \quad (17)$$

with the random values  $\gamma_i^{\text{pl}}$  being the center position of parabolae of curvature  $\tilde{\mu}$ , representing a disorder potential. This alternative description turns to be almost identical to the standard EPMS if we replace the parabolic

Table I. Values of the  $\beta$  exponent according to Eq. 18 for different models: Prandtl-Tomlinson (PT), Hébraud-Lequeux (HL) and the universe of  $2d$  EPMS.

Rate type	PT	HL	2d-EPM
	( $H=1$ )	( $H=1/2$ )	( $H=2/3$ )
Uniform	1	2	3/2
Progressive	3/2	5/2	2

potentials of Ref. [12] by piecewise potentials composed by flat regions (where the  $n = 1$  takes place) and ‘traps’ (where the  $n = 0$  and the local plastic deformation does not increase). The sole important analytical property of those traps would be their point of maximum slope, identified with the local yield threshold. The replacement of such a piecewise trap potential by a concatenation of parabolae in our argumentation is an additional allowance to forge the analogy among EPMS and depinning-like models. Now, accepting this analogy, we can test our data against the result for the stochastically driven Prandtl-Tomlinson model[24] (a mean-field version of Eq.17) for which it is analytically found that  $H$  and the flow exponent  $\beta$  are related by

$$\beta = 1 + \frac{1}{H} - \frac{1}{\omega}. \quad (18)$$

Simply replacing  $\mu = \frac{1}{H}$  in (14) using the above equation, leads to Eq. 16.

The values of  $\beta$  according to this formula for different values of  $H$  are summarized in Table I. The case  $H = 1$  corresponds essentially to the absence of stochastic noise, and this is realized in the standard one-particle Prandtl-Tomlinson model. In this case the values of  $\beta$  are well known. The value  $H = 2/3$  was argued before to correspond to the  $2d$ -EPM, and we observe in fact that the values on Table I are exactly the flow exponents that were obtained from the numerical results in Fig.1. The case of Gaussian noise  $H = 1/2$  with uniform rates is known to correspond to the Hébraud-Lequeux model. The value  $\beta = 2$  obtained from Eq.18 in fact constitutes the well-known result from this model ( $n = 1/\beta = 0.5$ ) [13, 14]. To complete the verification of the values contained in Table I, which is to say, the accuracy of Eq. 18, it remains to consider the HL model for progressive rates. An analytical derivation of  $\beta = 5/2$  for that case is presented in the next Section (III G).

For completeness, in Table II we summarize the values of the exponent we have obtained in the numerical simulations of the present work.

### G. Progressive rates in the Hébraud-Lequeux model

The Hébraud-Lequeux model [13] is defined by the evolution of the probability distribution function  $\mathcal{P}(\sigma, t)$  of local stress  $\sigma$  at time  $t$ , under an external strain rate  $\dot{\gamma}(t)$

Table II. Values of the critical exponents directly determined from the numerical simulations in two-dimensional systems. Exponents in general do not depend on the particular model analyzed. Dynamical exponents  $\beta$  and  $z$  differ for uniform and progressive rate rules.

	uniform	progressive
$\beta$	$1.5 \pm 0.1$	$2.0 \pm 0.1$
$\theta$ (from $(x_{\min})$ )	$0.5 \pm 0.05$	$0.5 \pm 0.05$
$\theta$ (from $P(x)$ )	$0.75 \pm 0.07$	$0.75 \pm 0.07$
$\tau$	$1.33 \pm 0.03$	$1.33 \pm 0.03$
$d_f$	$1.08 \pm 0.05$	$1.08 \pm 0.05$
$H$	$0.67 \pm 0.03$	$0.67 \pm 0.03$
$z/d_f$	$0.54 \pm 0.02$	$0.43 \pm 0.04$
$z$	$\sim 0.583$	$\sim 0.464$

as

$$\partial_t \mathcal{P}(\sigma, t) = -G_0 \dot{\gamma}(t) \partial_\sigma \mathcal{P} + D_{\text{pl}}(t) \partial_\sigma^2 \mathcal{P} - \nu(\sigma, \sigma_c) \mathcal{P} + \Gamma(t) \delta(\sigma) \quad (19)$$

where the rate  $\nu$  is given by

$$\nu_{\text{HL}}(\sigma, \sigma_c) \equiv \frac{1}{\tau} \theta(\sigma - \sigma_c) \quad (20)$$

(with  $\theta$  the Heaviside function and  $\delta$  the Dirac distribution) i.e., the rate of plastic events is approximated by a fixed value  $1/\tau$  in any overstressed region, and the plastic activity is defined from

$$\Gamma(t) = \frac{1}{\tau} \int_{\sigma' > \sigma_c} d\sigma' \mathcal{P}(\sigma', t), \quad (21)$$

Finally, a key ingredient of the model is that the diffusion coefficient  $D_{\text{pl}}(t)$  is assumed to be proportional to the plastic activity:

$$D_{\text{pl}}(t) = \tilde{\alpha} \Gamma(t) \quad (22)$$

where  $\tilde{\alpha} > 0$  is an ad-hoc parameter of the model. In a stationary situation, as the plastic activity is proportional to  $\dot{\gamma}$ , the previous equation also implies that  $\dot{\gamma} \sim D_{\text{pl}}$ . For any  $\tilde{\alpha}$  smaller than a critical value  $\tilde{\alpha}_c = \frac{\sigma_c^2}{2}$ , a non-trivial solution exist for the (nonlinear) evolution in  $\mathcal{P}(\sigma, t)$  that translates in a flowcurve ( $\langle \sigma \rangle = \sigma_c + A \dot{\gamma}^n$ ) with  $n = 1/2$  (i.e.,  $\beta = 2$ ).

In the following we will show that modifying Eq.(20) to

$$\nu(\sigma, \sigma_c) \equiv \frac{1}{\tau} (\sigma - \sigma_c)^k \theta(\sigma - \sigma_c) \quad (23)$$

i.e., introducing a stress-dependent progressive rate in the HL model, the flowcurve results in

$$\langle \sigma \rangle = \sigma_c + A \dot{\gamma}^{\frac{1}{2+k}} \quad (24)$$

Rather than attempting a full solution of Eq.(19) with the modified rate (23), we simply concentrate in tracking the impact of the functional form of the local plastic rate

in the scaling properties of the stress close to the critical point. First, notice that the result  $\dot{\gamma} \sim D_{\text{pl}}$  at first order [14] is still valid in this case. At the same time, the stress excess  $\Delta\sigma \equiv \sigma - \sigma_c$  when we impose a small strain rate is proportional to the probability density at the local threshold  $\mathcal{P}(\sigma_c)$ .

Looking for a stationary solution of Eqs. (19,23) at zero order in  $\dot{\gamma}$ , we can write for  $\sigma > \sigma_c$

$$0 = D \partial_\sigma^2 \mathcal{P} - (\sigma - \sigma_c)^k \mathcal{P} \quad (25)$$

The solution for  $\mathcal{P}$  should have the form

$$\mathcal{P} = \mathcal{P}(\sigma_c) f\left(\frac{\sigma - \sigma_c}{D^{\frac{1}{k+2}}}\right) \quad (26)$$

with  $f(0) = 1$ . Now, asking for the usual closure equation of the HL model (22) that provides self-consistency, we obtain

$$D = \tilde{\alpha} \frac{1}{\tau} \int_{\sigma' > \sigma_c} d\sigma' (\sigma' - \sigma_c)^k \mathcal{P}(\sigma') \quad (27)$$

$$= \tilde{\alpha} \mathcal{P}(\sigma_c) \int_{\sigma' > \sigma_c} d\sigma' (\sigma' - \sigma_c)^k f\left(\frac{\sigma' - \sigma_c}{D^{\frac{1}{k+2}}}\right) \quad (28)$$

$$= \tilde{\alpha} \mathcal{P}(\sigma_c) D^{\frac{k+1}{k+2}} \int_{u_0} du u^k f(u) \quad (29)$$

The last integral is just a number, then we conclude that

$$D \sim \mathcal{P}(\sigma_c) D^{\frac{k+1}{k+2}} \quad (30)$$

and

$$\Delta\sigma \sim \mathcal{P}(\sigma_c) \sim D^{\frac{1}{k+2}} \sim \dot{\gamma}^{\frac{1}{k+2}} \quad (31)$$

In other words,

$$\dot{\gamma} \sim (\sigma - \sigma_c)^{k+2} \quad (32)$$

for the HL model modified with progressive rates for local yielding of the form  $\sim (\sigma - \sigma_c)^k$ . In the particular case corresponding to smooth potentials we must take  $k = \frac{1}{2}$ , obtaining  $\beta = 5/2$  which is precisely the value predicted by Eq. (18) for this case.

#### IV. SUMMARY AND DISCUSSION

In this paper we have investigated different versions of elasto-plastic models (EPMs) discussed in the literature addressing their critical properties at the yielding transition. Accurate numerical simulations have revealed that for the three cases analyzed the critical exponents are the same, thus suggesting that these values are universal, independent of model details. Nevertheless, we have identified a dynamical rule in EPMs on which dynamical critical exponents depend upon. This is the form of the rate law used to fluidize sites that have exceeded the local yielding threshold. Previous implementations of EPMs in the literature considered this rate  $\lambda$  to be a

constant, independent of the degree of overstress above the threshold value. We have gone beyond that, analyzing also the case of a progressive rate that depends on the degree of overstress, in particular  $\lambda \sim (\sigma_i - \sigma_{Y_i})^{1/2}$ . This change of dynamical rule has a strong effect on the flowcurve exponent  $\beta$  (which changes from  $\beta = 3/2$  to  $\beta = 2$ ) and the dynamical exponent  $z$ . The change of rule impacts in exactly the same manner on the three models analyzed. Furthermore, we have investigated also the effect of progressive rate in mean-field. For the well known Hébraud-Lequeux model the inclusion of progressive rates transforms the flowcurve exponent from the standard  $\beta = 2$  value to  $\beta = 5/2$  in the progressive case.

We have argued that there is an analogy between EPMS and models with continuous pinning potentials: a fix plastic activation rate in EPMS corresponds to a disorder potential with sudden changes of slope when passing from a plastic metastable state to another, while the progressive rate corresponds to a smooth transition between metastable states. In fact, the values of the dynamical exponents in this kind of model with continuous pinning potentials was shown [12] to reproduce exactly the phenomenology discussed here for EPMS. We believe that smooth pinning potentials are more akin to the real experiment. The exponent obtained for this case ( $\beta = 2 \Rightarrow n = 0.5$ ) is, in fact, closer to the typical value (within broad dispersion) found in the laboratory [7].

Recently, a generalized mean-field treatment was presented in two different but almost equivalent ways in [19, 20] and [6, 12, 24]. This construction can be characterized by the Hurst exponent of the mechanical noise signal that any site in the system feels as a consequence of the dynamical evolution of all other sites, propagated through the Eshelby elastic kernel (therefore, closer to EPMS than the HL model and its diffusive perturbation term). By assuming individual instantaneous ‘kicks’, Lin and Wyart [19] suggest that  $H = 1$  is the only possible physical value. Nevertheless, we argue that the value of  $H$  is non-trivial and, furthermore, dimension dependent. This is, allowing ourselves to consider an effective mechanical noise with exponent  $H$  that takes into account the effect of full avalanches and not only single sites, we could exactly describe within a “mean-field” approach the complete spatial dynamics for a system in any dimension, as soon as the corresponding  $H$  is plugged in. For  $2d$  we obtain  $H \simeq 2/3$ , robustly in all tested models. Using this value and the analytical connection provided by the generalized mean-field treatment (Eq.18) we find  $\beta = 3/2$  for uniform rate, and  $\beta = 2$  for progressive rate, which nicely reproduce the results of full numerical simulations. We expect  $H$  to increase with dimension and  $\beta$  decrease towards the high dimension limit characterized by  $H = 1$ , and thus  $\beta = 1$  (uniform rates) or  $\beta = 3/2$  (progressive rates). In fact, in preliminary simulations in  $3d$  we have obtained  $\beta \simeq 1.3$  (uniform rates) and  $\beta \simeq 1.8$  (progressive rates).

Another exponent for which the generalized mean-field approach makes an accurate statement is the pseudo-gap

exponent  $\theta$ . If  $\beta > 1$ ,  $\theta = \beta/2$  is deduced. Considering it valid for the uniform rate EPMS and then using  $\beta = 3/2$ ,  $\theta = 3/4$  is obtained. This prediction of mean-field theory refers to the form of  $P(x) \sim x^\theta$  and we have found in simulations that  $\theta \simeq 0.75$  is indeed a good approximation for all three EPMS in both of their variants. Yet, as we have pointed out, the value of  $\theta$  obtained from the finite size scaling of  $\langle x_{\min} \rangle$  does not coincide with the prediction  $\theta = \beta/2$ . Certainly, the discordance between the two possible definitions of  $\theta$  deserves further investigation.

The finding of certain critical exponents ( $\beta, z, \delta$ ) depending on microscopic details of the disorder potential for the yielding transition has arisen somehow as a surprise, since it is commonly expected (based in the evidence provided by renormalization group arguments for the depinning transition) that these microscopic details should be irrelevant. A second thought, however, shows that this influence of dynamical rules that we observe in yielding is analogous to the one observed in depinning in the mean-field fully-connected case, where exponents depend on the particular shape of the disordered potential (see for instance [25]). Actually, the elastic coupling  $G_{\mathbf{q}}$  for yielding (Eq. 5) is in fact independent of the absolute value of  $\mathbf{q}$  (exactly as in the fully interacting depinning case, where  $G_{\mathbf{q}} = -\kappa$ , with  $\kappa$  a constant), generating a long range interaction in real space  $G(r) \sim 1/r^d$ . This ‘sorority’ between the yielding transition of amorphous solids and the fully-connected mean-field depinning classical problem is subject of analysis of a separate work [26].

## ACKNOWLEDGMENTS

EEF acknowledges support from grant PICT 2017-1202, ANPCyT (Argentina).

### Appendix A: Avalanche duration vs. size in mean-field

A toy model with discrete pinning sites and stress dependent transition rates can be used to investigate analytically the dependence between duration and spatial extent of avalanches. Imagine a pinning potential consisting of narrow wells in which an elastic interface is pinned. Each well has a threshold force value that is necessary to apply to unlock the interface from it. Once a local threshold is exceeded the interface locally jumps to the next well with probability  $\lambda$  (the inverse of the time it will take a particle to move from one well to the next).  $\lambda$  may be a constant or a quantity depending on the force excess over the threshold:  $\lambda = (f_i - f_i^{th})^\alpha$ , where  $f_i$  is the actual value of the force applied at site  $i$ ,  $f_i^{th}$  is the local threshold force, and  $\alpha$  is a numerical exponent. A configuration of the system is characterized by the values of  $f_i$ , which are the elastic forces at every site. The configuration is stable if  $f_i < f_i^{th}$ . On this configuration an avalanche is triggered by increasing uniformly the force

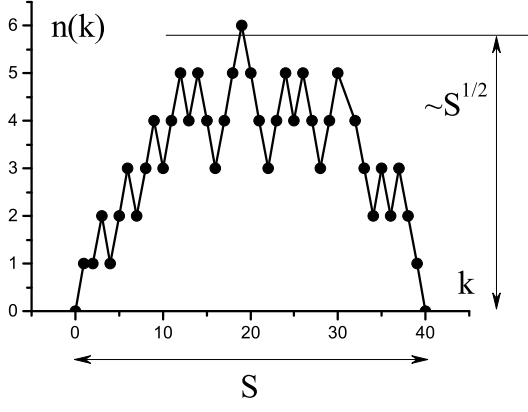


Figure 10. Instantaneous size of the avalanche as a function of the number of particles that already jumped to new equilibrium positions. This plot is a random walk. The duration  $T$  of the avalanche can be evaluated once the times  $dt_k$  to pass from  $k$  to  $k+1$  are known.

up to the point where  $f_i$  becomes equal to  $f_i^{th}$  at some particular  $i$ , which then becomes unstable. After some time the unstable site jumps to the next well,  $f_i$  is reduced by some quantity  $\delta$ , and all  $f_j$  move up a quantity  $\delta/N$ . This may produce some new sites to become unstable (i.e., to overpass their  $f^{th}$ ). The process continues until there are no more unstable sites. At this point an avalanche of some duration  $T$  and some spatial extent  $S$  has occurred.

We can obtain the relation between  $T$  and  $S$  for this avalanche as follows. Suppose we plot the number of unstable sites  $n$  as a function of the number of sites  $k$  that have already jumped to their new positions within the avalanche. Such a plot is a random walk. The avalanche size  $S$  is the number of sites that have jumped when there are no more unstable sites, namely  $n(S) = 0$ .

In order to calculate  $T$  for a given  $S$  we have to sum all time intervals  $dt_k$  between successive values of  $k$ , namely

$$T = \sum_{k=1}^{S-1} dt_k \quad (\text{A1})$$

Let us consider first the simplest case in which  $\lambda$  is constant. This means that any individual site jumps in a time that is always  $\sim 1$ . If there are  $n(k)$  unstable sites at some moment, the typical time for the first one of them to jump is  $dt_k \sim 1/n(k)$ . In addition, the average form of  $n(k)$  for a random walk between two zero crossings at 0 and  $S$  is  $n(k) \sim \sqrt{k(S-k)}/L^{1/2}$  then we obtain

$$T \sim \sum_{k=1}^{S-1} \frac{S^{1/2}}{\sqrt{k(S-k)}} \quad (\text{A2})$$

that for sufficiently large avalanches can be written (using

$x \equiv k/S$ ) as

$$T \sim \sum_{x=\frac{1}{S}, \frac{2}{S}, \dots, 1-\frac{1}{S}} \frac{S^{-1/2}}{\sqrt{x(1-x)}} = S^{1/2} \int_0^1 \frac{dx}{\sqrt{x(1-x)}} \propto S^{1/2} \quad (\text{A3})$$

i.e., we obtain  $z = 1/2$  which is the standard value of the dynamical exponent for depinning in mean-field.

The previous calculation can be extended to the case of an arbitrary value of  $\alpha$  in  $\lambda = (f_i - f_i^{th})^\alpha$ . It requires the evaluation of  $dt_k$  in this situation. The calculation is now non-trivial, because every unstable site has a different value of  $y_i \equiv f_i - f^{th}$ , and then a different transition rate. The value of  $dt_k$  is calculated as

$$dt_k = \left( \sum_{i=1}^{n_k} y_i^\alpha \right)^{-1} \quad (\text{A4})$$

(note that if  $\alpha = 0$ ,  $dt_k = 1/n(k)$  and we return to the previous case). To calculate  $dt_k$  the actual distribution of  $y_i$  values if needed. We focus on its calculation now.

Consider a situation with  $n$  unstable sites with values  $y_1 \dots y_n$ . We will work in a continuum limit, with  $n$  large. We want to calculate the expected distribution of  $y$ , that will be characterized by a function  $P(y)$ , such that

$$\int_0^\infty P(y) dy = n. \quad (\text{A5})$$

As the rate goes as  $y^\alpha$ , we can write

$$\frac{dP}{dt} = P y^\alpha \quad (\text{A6})$$

The equilibrium condition for  $P(y)$  is that when one of the  $y_i$  jumps (and then disappears as an unstable site) and all the distribution is shifted by  $1/N$  the configuration remains stable. This leads to

$$\frac{dP}{dt} = C_0 \frac{dP}{dy} \quad (\text{A7})$$

The constant  $C_0$  remains yet undetermined, and will be fixed by normalization below. Combined with the previous equation this gives

$$C_0 \frac{dP}{dy} = P y^\alpha \quad (\text{A8})$$

and from here

$$P(y) = P_0 \exp\left(-\frac{C_0 y^{\alpha+1}}{\alpha+1}\right) \quad (\text{A9})$$

The two constants are determined from the normalization condition (Eq. A5), and from the fact that  $P(0) = N$ , since on average, a shift in  $y$  of  $1/N$  produces the appearance of one new unstable site. The final result is

$$P(y) = N \exp\left[-a_0 \left(\frac{Ny}{n}\right)^{\alpha+1}\right] \quad (\text{A10})$$

with  $a_0$  a numerical constant. The continuous form of Eq. (A4) allows to calculate the average time interval up to the next particle jump  $dt_k$  as

$$dt_k = \left( \int_0^\infty P(y) y^\alpha dy \right)^{-1} \quad (\text{A11})$$

Doing the integration, the result is

$$dt_k \sim \frac{N^\alpha}{n^{\alpha+1}} \quad (\text{A12})$$

Using this expression to perform the same analysis that was done before in Eqs. (A2), (A3) leads to (assuming  $\alpha < 1$ )

$$T \sim \sum_{k=1}^S \frac{N^\alpha S^{(\alpha+1)/2}}{(k(S-k))^{(\alpha+1)/2}} \quad (\text{A13})$$

$$T \sim \sum_{x=\frac{1}{S}, \frac{2}{S}, \dots, 1-\frac{1}{S}} \frac{N^\alpha S^{-(\alpha+1)/2}}{(x(1-x))^{(\alpha+1)/2}} \sim N^\alpha L^{(1-\alpha)/2} \quad (\text{A14})$$

This is the final result. It provides the value of the dynamical exponent as  $z = (1 - \alpha)/2$  and, at the same time, a dependence on the system size  $N$ . The latter disappears in the uniform rate case ( $\alpha = 0$ ), corresponding to cuspy potentials.

- 
- [1] S. Karmakar, E. Lerner, and I. Procaccia, *Phys. Rev. E* **82**, 055103 (2010).
- [2] J. Lin, E. Lerner, A. Rosso, and M. Wyart, *Proceedings of the National Academy of Sciences* **111**, 14382 (2014).
- [3] B. Tyukodi, S. Patinet, S. Roux, and D. Vandembroucq, *Phys. Rev. E* **93**, 063005 (2016).
- [4] M. Ozawa, L. Berthier, G. Biroli, A. Rosso, and G. Tarjus, *Proceedings of the National Academy of Sciences* **115**, 6656 (2018).
- [5] A. Nicolas, E. E. Ferrero, K. Martens, and J.-L. Barrat, *Rev. Mod. Phys.* **90**, 045006 (2018).
- [6] E. A. Jagla, *Phys. Rev. E* **96**, 023006 (2017).
- [7] D. Bonn, M. M. Denn, L. Berthier, T. Divoux, and S. Manneville, *Rev. Mod. Phys.* **89**, 035005 (2017).
- [8] G. Picard, A. Ajdari, F. Lequeux, and L. Bocquet, *The European physical journal. E, Soft matter* **15**, 371 (2004).
- [9] G. Picard, A. Ajdari, F. Lequeux, and L. Bocquet, *Physical Review E* **71**, 010501 (2005).
- [10] A. Nicolas, J. Rottler, and J.-L. Barrat, *The European Physical Journal E* **37**, 50 (2014).
- [11] C. Liu, E. E. Ferrero, F. Puosi, J.-L. Barrat, and K. Martens, *Phys. Rev. Lett.* **116**, 065501 (2016).
- [12] I. Fernández Aguirre and E. A. Jagla, *Phys. Rev. E* **98**, 013002 (2018).
- [13] P. Hébraud and F. Lequeux, *Physical Review Letters* **81**, 2934 (1998).
- [14] E. Agoritsas, E. Bertin, K. Martens, and J.-L. Barrat, *Eur. Phys. J. E* **38**, 71 (2015).
- [15] M. Talamali, V. Petäjä, D. Vandembroucq, and S. Roux, *Physical Review E* **84** (2011).
- [16] Z. Budrikis, D. F. Castellanos, S. Sandfeld, M. Zaiser, and S. Zapperi, *Nat. Comm.* **8**, 15928 (2017).
- [17] E. A. Jagla, *Phys. Rev. E* **92**, 042135 (2015).
- [18] C. Maloney and A. Lemaitre, *Physical Review Letters* **93**, 016001 (2004).
- [19] J. Lin and M. Wyart, *Physical Review X* **6**, 011005 (2016).
- [20] J. Lin and M. Wyart, *Phys. Rev. E* **97**, 012603 (2018).
- [21] X. Cao, A. Nicolas, D. Trimcev, and A. Rosso, *Soft matter* **14**, 3640 (2018).
- [22] C. Schölzel, “Python nolds library,” <https://pypi.org/project/nolds/> (2018).
- [23] Notice that in a previous publication by one of us [12], the relation  $\theta = \frac{1}{H} - 1$  was proposed. However, the derivation of this relation was based on a wrong assumption. This relation is not correct.
- [24] E. Jagla, *Journal of Statistical Mechanics: Theory and Experiment* **2018**, 013401 (2018).
- [25] A. B. Kolton and E. A. Jagla, *Phys. Rev. E* **98**, 042111 (2018).
- [26] E. E. Ferrero and E. A. Jagla, “Elastic interfaces on disordered substrates: From mean-field depinning to yielding,” In preparation (2019).